

Quantitative Ultrasound Spectroscopy for Screening Cylindrical Lithium-Ion Batteries for Second-Life Applications

Simon Montoya-Bedoya,^[a, b] Esteban Garcia-Tamayo,^[d] Daniel Rohrbach,^[c] Juan Pablo Gaviria-Cardona,^[b] Hader V. Martinez-Tejada,^[b] Brady Planden,^[e] David A. Howey,*^[e] Whady F. Florez,^[b] Raúl A. Valencia,^[b] and Miguel Bernal^[c]

Diagnosing lithium-ion battery degradation is a crucial part of managing energy storage systems. Recent research has explored ultrasonic testing for non-invasive health assessment as an alternative to traditional, time-consuming, electrical-only methods. Assessing the state of health is vital for determining quality at end of 'first' life, with retired batteries at 70–80% health still holding value for secondlife applications. Over the coming years, tens of GWh of salvaged batteries will hit the market, requiring rapid noninvasive methods to classify retired batteries according to their state of health. This study uses a 64 – element ultrasonic array to obtain mid-band quantitative ultrasound spectroscopy parameters – including mid-band fit,

spectral slope, and intercept – from circumferential waves around cylindrical batteries. Thirteen cylindrical cells were used to evaluate the methodology: three pristine and ten retired from the same source. The mid-band fit showed the ability to track the state of charge and discriminate between the state of health levels in accelerated degradation experiments both with pristine batteries, and also with recovered secondlife batteries with unknown historical use. Linear-array ultrasonic transducers, coupled with quantitative spectral parameters, show promise for future non-destructive battery health screening methods, offering valuable insights for the emerging used battery market.

Introduction

Interest in energy storage systems has increased due to their key role in the race against climate change.^[1] Lithium-ion batteries (LIBs) have become the main energy storage technology for electric vehicles (EVs), because of their high energy density,^[2,3] and for stationary storage applications, as they

compensate for the variable nature of renewable energy generators. These technologies are rapidly increasing their share of the global energy mix and are helping to bring electricity to off-grid communities.^[4]

The growing trend for LIBs has emphasized the need for a holistic view of their value chains^[5] including battery manufacturing, primary application, battery re-purpose, second-life applications, recycling, and final disposal.^[5,6] Since batteries are high-value assets, we must maximize the extraction of value from them during life and adopt circular economy frameworks to reduce the generation of waste and improve the use of valuable resources.^[7,8] The end of life for LIBs in electric vehicles is reached at approximately 70–80% of their State of Health (SOH) (defined as the remaining percentage of the capacity compared to the pristine state)^[9] because this has been defined as a point where batteries would not satisfy the mobility needs of consumers.^[10] This threshold has been revised by some authors,^[11,12] but, regardless, retired LIBs from EVs present substantial opportunities for repurposing as second-life batteries (SLBs) in lower power demand applications.^[13] Such life extension reduces the pressure to mine high-value and hard-to-extract minerals used to manufacture new LIBs, and further avoids early recycling.^[14,15] Conventionally, cell-to-cell variations within a module of a retired EV battery pack necessitate individual SOH assessments to ascertain suitability for repurposing as SLBs. Research has explored the prospective advantages and barriers associated with SLBs,^[16,17] as well as the criteria for sending cells directly to recycling.^[18]

Conventional battery SOH or State of Charge (SOC) estimation methods require performance and internal changes

[a] *S. Montoya-Bedoya*

Verasonics SAS
Cq. 1 #70-01 Bl. 11 Of. 511, Medellin, 50031, Colombia

[b] *S. Montoya-Bedoya, J. P. Gaviria-Cardona, Prof. H. V. Martinez-Tejada, Prof. W. F. Florez, Prof. R. A. Valencia*

School of Engineering
Universidad Pontificia Bolivariana
Cq. 1 #70-01, Medellin, 50031, Colombia

[c] *Dr. D. Rohrbach, Dr. M. Bernal*

Verasonics Inc.
11335 NE 122nd Way, Kirkland, WA 98034, United States

[d] *Dr. E. Garcia-Tamayo*

BATx SAS
Cra. 45 #31–49, Medellin, Colombia

[e] *Dr. B. Planden, Prof. D. A. Howey*

Department of Engineering Science
University of Oxford
Parks Road, Oxford, OX1 3PJ, United Kingdom
E-mail: david.howey@eng.ox.ac.uk

 Supporting information for this article is available on the WWW under <https://doi.org/10.1002/batt.202400002>

 © 2024 The Authors. *Batteries & Supercaps* published by Wiley-VCH GmbH. This is an open access article under the terms of the Creative Commons Attribution License, which permits use, distribution and reproduction in any medium, provided the original work is properly cited.

to be inferred from external signals such as electrical measurements and surface temperature. The estimation of health for SLBs is a complex task due to the different degradation pathways a retired battery may have suffered.^[19,20] Nonetheless, accurate SOH estimation is required to ensure the continued safe and correct operation of the SLBs,^[14,21] and the methods to achieve this need to be relatively fast.^[22] Standard capacity measurements for SOH estimation, using techniques such as Coulomb counting, are time-consuming due to the low applied currents, and are therefore impractical for use in high throughput scenarios.^[23] A challenge also arises from the absence of historical usage data, requiring additional tests to characterize the LIBs to account for the different degradation pathways that they might have undergone during their first life.^[24,25] Recent research has focused on developing rapid and non-destructive evaluation (NDE) techniques for battery state estimation, such as X-ray Computed Tomography (X-ray CT),^[26–28] Electrochemical Impedance Spectroscopy (EIS)^[29–32] and acoustic methods.^[33–35] The versatility and relatively low cost of ultrasound equipment compared to other NDE techniques has stimulated research using various acoustic approaches for SOC and SOH estimation purposes.^[36–39] In addition, since ultrasound wave propagation is directly influenced by changes in the mechanical properties within the specimens tested, it can give insight into a battery's internal state.^[40,41]

Ultrasound was introduced for SOH monitoring of LIBs in Ref. [42], who observed a decrease in the amplitude of an ultrasound transmission signal when comparing the cycled state to the original battery state. The authors suggested that these observations could be associated with degradation due to gas evolution, electrode expansion, and other mechanisms. Research reported in Refs. [37,43] demonstrated the connection between ultrasound and battery state and showed that the SOC and SOH have an impact on the amplitude and the time of flight (ToF) of ultrasonic waves propagating through the batteries. Some other studies have also used the ToF as an indicator of SOC changes and also as a health indicator.^[44–47] These relationships between battery state and ultrasound signal characteristics have been explained by the evolution of mechanical properties. Changes in the bulk modulus, shear modulus, and density changes of the cell stack (a layered structure within the battery) during the charge and discharge phases of the LIBs are a result of the lithiation and delithiation of the electrodes.^[48–50] In fact, it has been shown that changes in the graphite negative electrode and the graphite/electrolyte interface dominate the ultrasonic response of the battery, as the changes in the positive electrode material and thickness are negligible compared to that of the anode.^[51]

Most literature has focused on analyzing waves that propagate throughout the flat, layered structure of pouch-type LIBs. However, alternative methodologies, such as guided waves, leverage the battery geometry as a waveguide, thereby minimizing energy loss and covering a substantial portion of the surface area.^[38,52] This work reported an inverse linear relationship between the ToF and the SOC and the authors also observed a shift towards lower ToF and higher amplitude of the ultrasonic guided waves as a function of the number of charge/

discharge cycles during aging. Moreover, recent studies have correlated different characteristics of guided waves to the battery state.^[53–55] It should be noted that guided waves often operate at lower frequencies than compression waves, and are well suited to prismatic and pouch form factors.^[56]

Cylindrical LIBs are widely used in consumer electronics and have gained significant traction in the automotive industry, particularly with Tesla's announcement of the cylindrical 4680 format.^[57] The challenge of recycling these is pronounced due to the complexity of separating electrodes from their tightly coiled structure.^[58] This highlights the need for rapid, non-destructive techniques to evaluate the SOH of cylindrical cells, where one promising approach is ultrasonic testing. However, the unique 'jelly roll' configuration and the rigid stainless steel casing of cylindrical cells pose distinctive challenges for ultrasound propagation, as demonstrated by a limited body of research.^[43,59,60] Thus, we aim to bridge the gap in knowledge and explore the potential of ultrasonic testing for cylindrical geometries in pursuing non-destructive and rapid methods that enable second-life markets.

Ultrasound signal characteristics in both the time and frequency domain^[61,62] are useful as health indicators for SOH assessment. Nevertheless, the majority of previous studies have been carried out with batteries cycled in a laboratory environment and have not explored the use of ultrasound characteristics as quick tests to classify SLBs from the field in terms of their SOH, as evidenced by the limited existing research.^[63] Here we address the primary challenge of the widespread adoption of ultrasound technologies in assessing the SOH, which is the extension of these techniques for batteries with an unknown usage history, as highlighted in recent literature.^[14] We explore the potential of Quantitative Ultrasound Spectroscopy (QUS) as a novel metric for SOH assessment in cylindrical SLBs batteries with unknown histories, drawing inspiration from biological applications, where tissue characterization using quantitative ultrasound is widely and effectively employed. This spectral-based (frequency domain) method seeks to extract quantitative parameters that are related to physical properties.^[64] Prostate cancer detection and classification,^[65] and thyroids^[66] are a few examples. In the current work, QUS was studied with pristine batteries subject to accelerated degradation and then extended to explore its implementation as a fast screening framework for cylindrical SLBs with an unknown degradation path. Finally, the potential application of this method to C-rate varying scenarios, such as when a battery is operating in an EV (i.e. under drive cycle conditions), was also explored as it has only been investigated by a few researchers.^[45,67] To the authors' knowledge, this is the first time reported in the literature where an ultrasound methodology has been directly applied to recovered SLBs.

The main contributions of the present study can be summarized as:

1. The introduction of QUS for use as a non-invasive technique to extract spectral parameters that could be used as health indicators for LIBs and SLBs.

2. Investigation of an ultrasound methodology with cylindrical geometry batteries, which have a more complex wave propagation path compared to other flat geometries.
3. Exploration of the QUS methodology with batteries submitted to accelerated degradation and extending frequency ultrasound characteristics for screening of SLBs according to their SOH.
4. Evaluation of the spectral methodology on experiments under drive cycle conditions.

Results and Discussion

Ultrasound Wave Propagation

Ultrasonic waves propagating in cylindrical LIBs present more complex propagation paths compared to geometries such as pouch cells, as evidenced in previous studies.^[43] Both cylindrical and flat geometries consist of a multilayer structure of electrodes, metallic collectors, and separators immersed in a liquid electrolyte. A general equation for the propagation of ultrasonic waves in an elastic body can be found in Ref. [68], which is the model used by the simulation tool of this work. In addition, the interaction of ultrasonic waves with interfaces between material layers, each characterized by different acoustic impedances (Z), affects their propagation. In the case of compressional waves in

a general elastic body, these impedances can be described as a simplified version that depends on the density (ρ) and the elastic behavior of each material, characterized by the first and second Lamé elastic constants (λ, μ ; which are related to the stiffness tensor as shown in the Supporting Information),^[69] as outlined in Eq. (1). Charge and discharge processes involving lithiation or delithiation of the battery electrodes, along with degradation phenomena in aging batteries, modify the mechanical properties (and therefore Z) of the layers, consequently affecting the ultrasonic signals.^[52,67]

$$Z = \sqrt{\rho(\lambda + 2\mu)} \quad (1)$$

Current research has focused primarily on flat-structured batteries, leaving unresolved questions about ultrasound propagation inside cylindrical batteries. This form factor introduces unique interactions, influenced not only by geometry but also by mechanical deformation caused by the expansion of spirally coiled, elastic materials.^[70] Our initial assumption was that the correlations observed between the QUS parameters and the battery state originated from the backscattered signals of the back-wall reflections as they traveled through the battery. However, simulation studies conducted with the battery cross-section and media shown in Figure 1(a–b) (see Experimental section for details on simulation settings and materials properties) revealed the propagation of longitudinal circumferential

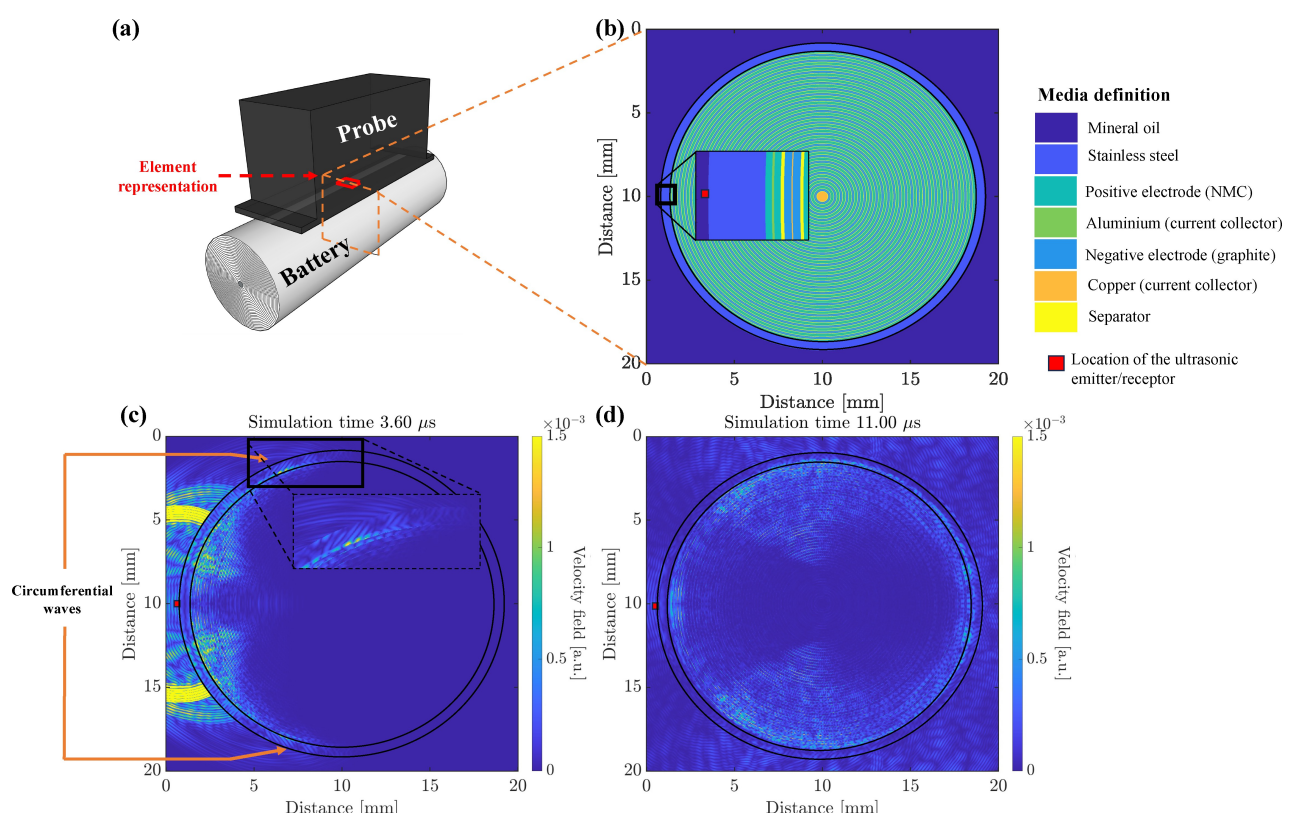


Figure 1. Diagram of the simulation performed to understand ultrasound wave propagation in cylindrical batteries under the conditions of this paper. (a) 3D render of the cylindrical battery aligned in a parallel orientation with the ultrasound array showing a unique element position used for the simulation with a red marker, (b) grid that represents the media used for simulation and (c,d) snapshots of the simulation results for the beginning of the circumferential wave propagation at two different timestamps. The snapshots were normalized between 0–0.0015 to increase contrast.

waves around the stainless-steel case, influenced by wave interactions with the internal layers. These ultrasonic waves carry information about the battery SOC and SOH. This finding aligns with the characteristic region identified in the ultrasonic experiments (Figure 8(a)). Given the cell diameter of 18.4 mm and circumferential perimeter of about 57.8 mm, echoes at $\sim 10 \mu\text{s}$ correspond to a sound speed of approximately $\sim 5780 \text{ m s}^{-1}$.

In Figure 1(c) and Figure 1(d), snapshots of the simulation illustrate the velocity field of the circumferential waves in the cell case. As they move, the circumferential waves receive information from the waves traveling in the internal layers near the battery case, which are affected by the internal battery materials, as shown in Figure 1(d), where the scattered waves due to the interaction with the internal layers can be observed. Previous studies have shown that wave propagation in cylindrically layered media is determined by scattering effects generated by the refractions and reflections at the interfaces of the internal layers and boundaries.^[71] Here, the simulation verified that these scattering effects from the internal layers contribute to the circumferential waves that were measured in a pulse-echo setup. We were interested in using pulse-echo to eliminate the additional complexity and alignment challenges of using two phase array transducers, as would be required in a pitch-catch setup. However, we will continue to explore this in future research.

We hypothesize that the wave interactions at the interfaces cause a change in the characteristics of the circumferential waves, which allows this ultrasonic testing technique to obtain information about the battery state. In addition, the potential influence of changes in cell thickness due to expansion and contraction on circumferential waves traveling in the case has been considered in light of the observed cell diameter variations during cycling, as discussed in Ref. [72]. While our preliminary analysis suggests that the quantitative parameters extracted here may be robust to these expansion/contraction changes within our current analysis window, future experiments involving coupled ultrasound measurements and detailed cell thickness assessments could provide a more comprehensive understanding, particularly in the context of potential aging effects. Furthermore, prior studies have examined ultrasonic methods in cylindrical structures like pipelines and fluid-filled shells, demonstrating the effectiveness of these techniques in gathering internal information from such structures.^[73,74]

Ultrasound propagation in intricate structures, like the “jelly roll” form of cylindrical batteries, presents significant complexities. The simulation employed in our study qualitatively elucidates the ultrasonic wave propagation mechanisms in cylindrical batteries under specific experimental conditions. It is important to note that while the simulation provides foundational insights, it does not account for the variation of mechanical properties, such as Lamé constants, across different SOC and SOH levels. These parameters are sensitive to operational conditions and their determination represents a significant challenge due to the lack of readily available data. Future research will aim to enhance the predictive capabilities of our ultrasonic assessment approach for cylindrical battery health

diagnostics by extending our simulation framework to incorporate dynamic mechanical properties and conducting further experimental and numerical studies for a comprehensive understanding of the underlying mechanisms. In this study, we focused on the analysis of circumferential wave signals, which have empirically shown the most promise for assessing battery state using the QUS parameters presented here. The Supporting Information (A.2) includes a simulation video, offering a more comprehensive view of the process.

Ultrasound for Battery Degradation Analysis

Pristine Batteries Submitted to Accelerated Degradation

Figure 2 presents the (a) voltage, (b) mid-band fit (MBf), (c) spectral slope (SS) and (d) 0 MHz intercept (I0) for the periodic reference performance tests (RPTs) during the accelerated degradation of one of the three pristine cells (see Figure C.2 and Figure C.3 in the supporting information for the results of the other two pristine cells tested). The SOH decreased from 100% to 83% after the 40 degradation cycles (see cycling data in the Supporting Information for further analysis). During charging, a gradual decrease can be observed in most of cases for the MBf and I0 until the constant voltage (CV) phase is reached, where an approximately constant value for both QUS parameters appears. Once discharge begins, MBf and I0 increase until coming back to the initial state.

The trends observed for SS during charge/discharge are more difficult to analyze due to the frequency dependency of this parameter. However, this metric may serve as an indicator of other phenomena occurring within the battery, and further investigation is needed to better understand the impact of SOH on the frequency dependence of the ultrasound spectrum. For example, a more sophisticated function fitted to the power spectrum may lead to better results. The MBf exhibits smoother curves compared to the behavior exposed by the SS and the I0, showing more potential to be used as an indicator for state assessment since it appears to be more consistent.

The SS follows a change in the frequency-dependent attenuation, however we did not identify a clear trend versus SOC and SOH for this parameter. On the other hand, MBf and I0 are connected to the ultrasonic signal amplitude changes because they are related to the amplitude damping or attenuation in the frequency domain. In this regard, some authors^[75,76] have reported a general increase in the rigidity of the battery during charging primarily due to the behavior of the graphite. Graphite undergoes a $\sim 10\%$ volume expansion and contraction during lithiation/delithiation and has a 3 times higher bulk modulus in the fully lithiated graphite (charged) state compared to the fully delithiated state (discharged), which is significantly higher compared to the positive electrode and other non-electrochemically active materials (such as collectors and the separator) within the battery. These characteristics have led to the consideration of graphite intercalation mechanics as the main contributor to the ultrasonic response of the battery.^[75] The changes in graphite stiffness alter its acoustic

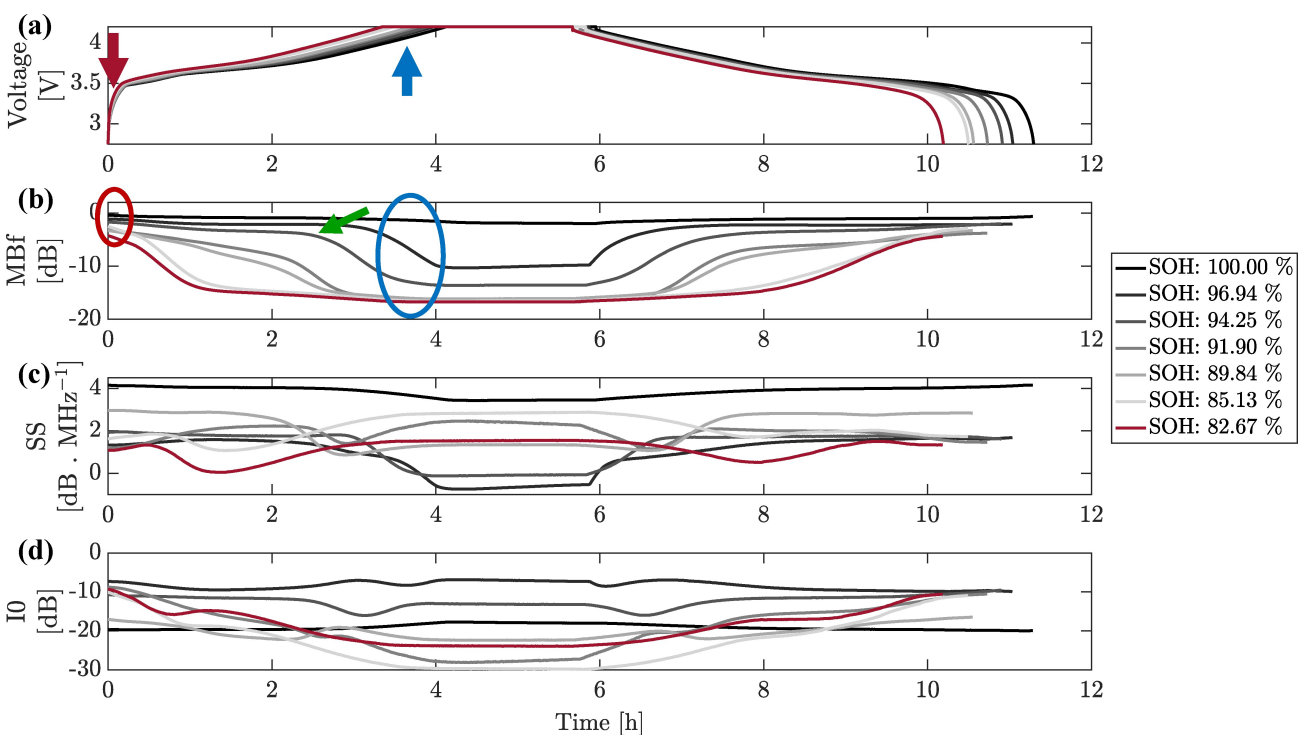


Figure 2. Results of accelerated degradation experiments in one cell showing (a) voltage, (b) MBf, (c) SS and (d) I₀ for different stages of degradation from 100% to 83% SOH.

impedance, affecting the mismatch of acoustic impedance at certain interfaces ("Cu | C", "C | separator", "separator | C" and "C | Cu"), and thus influencing how ultrasound scatters across these interfaces.^[41,62] Our results show that MBf, in particular, is affected by these changes as it tracks the charging and discharging (Figure 2).

Regarding the behavior of the QUS parameters during aging, Figure 2(b) shows that MBf can differentiate between different SOH levels following degradation cycling. Figure 2(c-d) show that, although both SOC and SOH affect SS and I₀, no clear trend can be observed – suggesting poor sensitivity of these two features for tracking SOC or SOH. Therefore, the remainder of this paper focuses on the MBf feature, which has clear potential to be used as a health indicator since it shows a trend towards lower amplitudes as the battery is degraded, going from -1.95 dB at the pristine state to -16.73 dB at about 83% SOH when the battery is at the full-charged state. The differences in MBf between the onset and the end of the constant current (CC) charge phase increase with battery degradation. Previous studies have focused on correlating SOC with ultrasonic parameters. However, literature is scarce in the evaluation of battery degradation in cylindrical geometry. One of the few studies that explored this geometry found challenges such as a cycle-by-cycle comparison of the reflected acoustic signal of an NCA/graphite cylindrical battery that did not show a clear trend.^[43]

Given the complexity of battery aging, which leads to diverse degradation mechanisms impacting the mechanical performance of the battery materials,^[20,77] understanding how these mechanisms influence ultrasound waves remains a key

area of research.^[78] We hypothesize that the decreasing trend in MBf values during the aging process is caused by higher attenuation of the ultrasonic signals within the internal layers of the battery. In this sense, several studies have shown structural changes in cylindrical lithium-ion batteries due to aging using X-ray CT techniques, where cylindrical LIBs suffer jelly roll deformation due to mechanical stresses induced in the structure during aging.^[79–81] Therefore, degradation can lead to less well defined structures, which may result in more scattering of the ultrasound signals. In addition, local variations in acoustic impedance will cause increased scattering, which together with absorption within the layers can cause attenuation of the ultrasonic signals. This will result in a lower amplitude of the circumferential waves due to scattering effects at the more heterogeneous internal interfaces.

The green arrow in Figure 2(b) points the reader to a feature that was observed in the accelerated degradation experiments for all the RPTs, where batteries with lower SOH exhibited a drop of the MBf at increasingly lower voltages during aging. This progressive change may be caused by lithium plating. Although LIBs undergo diverse degradation mechanisms, lithium plating has been reported as the most prevalent under the accelerated degradation conditions chosen, i.e., fast charge and low-temperature cycling.^[82] This characteristic of the ultrasonic signals could be correlated with the progressive deposition of metallic lithium on the negative electrode surface. Nevertheless, direct verification of lithium plating was not feasible in these experiments. Hence, the identification of lithium plating is reserved for future post-mortem analysis. Other studies using flat battery geometries have determined the amount of lithium

plating caused by cycling using ultrasonic ToF measurements.^[83]

Figure 3 shows a scatter plot of the MBf values obtained from seven RPTs conducted during the cycling of three batteries. The MBf data were extracted from two specific regions: the beginning of the charging phase or fully-discharged state (indicated by the Dch label with red markers, red-circled area in Figure 2(b)) and the end of the CC region in the charging phase (notated as Ch label with blue markers, blue-circled area in Figure 2(b)). A trend showing a lower amplitude of MBf was identified for all the cells as a function of degradation. A steeper slope above ~90% state of health was observed for the measurements from the end of the CC charge compared to the MBf values in the discharged state. Despite the expected variability between the MBf values measured for the cells at similar SOH levels, the consistent trends observed for the QUS parameter in both cases show the potential of this technique to be used as a rapid general metric to assess the health of a battery. In addition, as the results showed a higher sensitivity of the MBf at the upper cut-off voltage of 4.2 V, employing this method at high states of charge could be preferable to assess SOH.

Although previous studies have investigated the impact of temperature changes in LIBs on the propagation of ultrasound,^[67] the ultrasonic experiments in the current study were done at a low C-rate condition where the change in temperature was less than 1°C (as reported in Figure C.1(a), Figure C.2(a) and Figure C.3(a)) throughout the cycling process. Therefore, temperature did not significantly impact the ultrasound parameters, and the changes of the QUS parameters evidenced during the charge and discharge phases and with aging may be solely attributed to battery internal state changes.

Testing Second-Life Batteries

We now consider screening of SLBs after first life applications. The cells used were the same manufacturer and model as those used in the accelerated degradation experiments, and had

unknown historical usage. Results of cycling experiments on these cells are given in Figure 4, showing a subset of four representative batteries across a range of SOH values. Further details of the cycles for all ten batteries are given in Supporting Figure D.1. Overall, the measured state of health ranged from about 72% to 30%.

The measured MBf results for the SLBs have similar trends to those recorded for the lab experiments in the preceding section. Again, a correlation emerges between MBf and SOH. Despite the differences in the aging path, between the SLBs compared to those with a controlled cycling process,^[14] the MBf showed its robustness to follow the charge/discharge process. An evident correlation emerges between increased battery degradation and lower mid-band fit values, presumably linked to higher attenuation of the circumferential ultrasonic signals in more degraded batteries. The underlying physical reasons for these findings require additional testing and study to explain, such as *post-mortem* analysis with more ultrasonic testing to differentiate between the different degradation mechanisms presented.

Nonetheless, in contrast to other ultrasonic testing methods that try to decouple the ultrasonic response of the different battery layers,^[84,85] our approach centers on evaluating the entire response of the cylindrical battery as an integrated system. This offers valuable insights for rapid and non-invasive battery health evaluation, particularly in scenarios where expedited screening methods are indispensable.

We now compare (in Figure 5) the ultrasonic screening results for both the accelerated degradation cycled cells and the SLBs, and note that the mid-band fit analysis performed on second-life batteries appears to extend the patterns observed in the accelerated degradation experiments. The results in Figure 5 show a clear difference in the MBf for the "Ch" state compared to the "Dch" state. In the case of the "Dch" state, a more monotonic slope was observed for the MBf as a function of the SOH, while the "Ch" state shows at least two distinct rates above and below 90% SOH. An abrupt increase in MBf is observed between 90–100% for the "Ch" data, suggesting a potential transition between distinct regimes. However, below

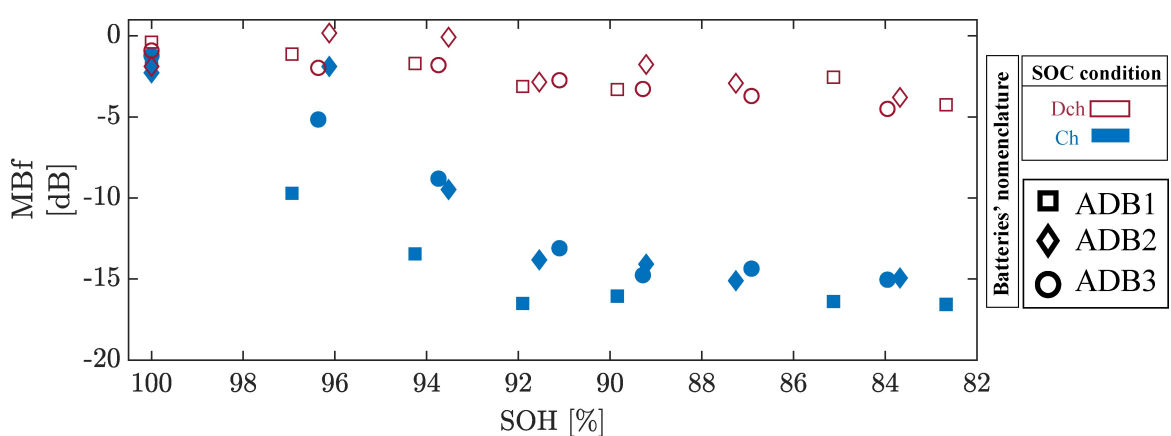


Figure 3. Relationship between the MBf and the SOH for measurements extracted at the onset of the charging phase ('Dch' in red) and the end of the CC region of the charge ('Ch' in blue) for three batteries submitted to accelerated degradation. ADB_i: Accelerated degraded battery i.

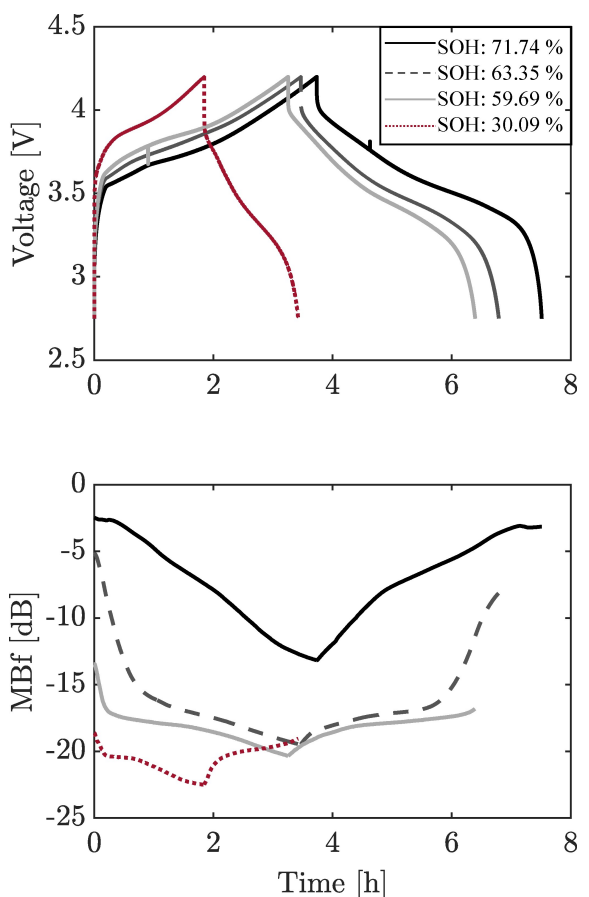


Figure 4. Results from the 1st cycle of the experiments performed with second-life batteries: (a) voltage measured and (b) MBf calculated from ultrasonic acquisition during the charge/discharge process. To enhance clarity, a subset of representative curves is displayed – the complete dataset of batteries is available in Supporting Figure D.1.

90%, the “Dch” data may provide more insightful information to determine the SOH of a certain SLBs.

To illustrate how the QUS methodology could be used for health assessment, fifth-order polynomials were fitted to the MBf vs. SOH values in the “Dch” and “Ch” cases (mathematical expressions are given in Supporting Information E). Despite the unknown degradation pathways^[19] and usage histories of the second-life batteries, our methodology exhibits the potential to offer robust SOH assessments, irrespective of the specific degradation mechanisms experienced and even when historical usage data is not available.

Extending Ultrasound Analysis to Real-Scenario Testing

In addition to investigating QUS as a screening method, we conducted a preliminary exploration of the technique in scenarios with variable operating C-rates, typical in EVs. Here, batteries rarely undergo constant applied current; instead, the current fluctuates during accelerating, decelerating, or maintaining a constant velocity.^[86] Furthermore, the battery can abruptly switch between charging and discharging at irregular rates. For this technology to be applicable in EVs and potentially in SLBs scenarios, the system must reliably track the battery’s SOC even under varying these varying conditions. To determine the method’s ability to function under varying conditions, ultrasonic measurements were taken during a drive cycle discharge test, as shown in Figure 6 for (a) a pristine battery, (b) an aged battery after the accelerated degradation process, and (c) one of the SLBs.

Figure 6 demonstrates the ability of the MBf to respond quickly to dynamic changes in state of charge and state of health in the three batteries tested with a drive cycle. The SLB and the battery post-accelerated degradation exhibited a higher variation in MBf in response to abrupt current changes, whereas the pristine battery showed a smaller magnitude of changes in MBf (the differences between the MBf at the start and the end of the process were $\Delta=0.57$ dB, $\Delta=6.49$ dB and $\Delta=5.50$ dB for the pristine battery, the aged battery after the accelerated degradation and the SLB, respectively). This

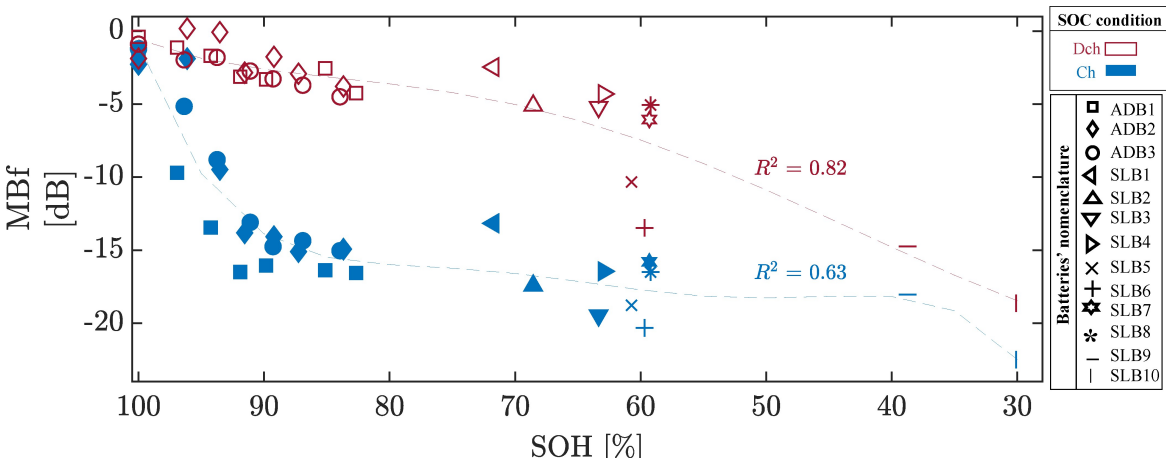


Figure 5. Relationship between the MBf and the SOH for measurement extracted at the onset of the charging phase (“Dch” in red) and the end of the CC region of the charge (“Ch” in blue) for the three batteries submitted to accelerated degradation and ten second-life batteries tested. Polynomial fits were adjusted in both cases to construct calibration curves. ADBi: Accelerated degraded battery i. SLBi: Second-life battery i.

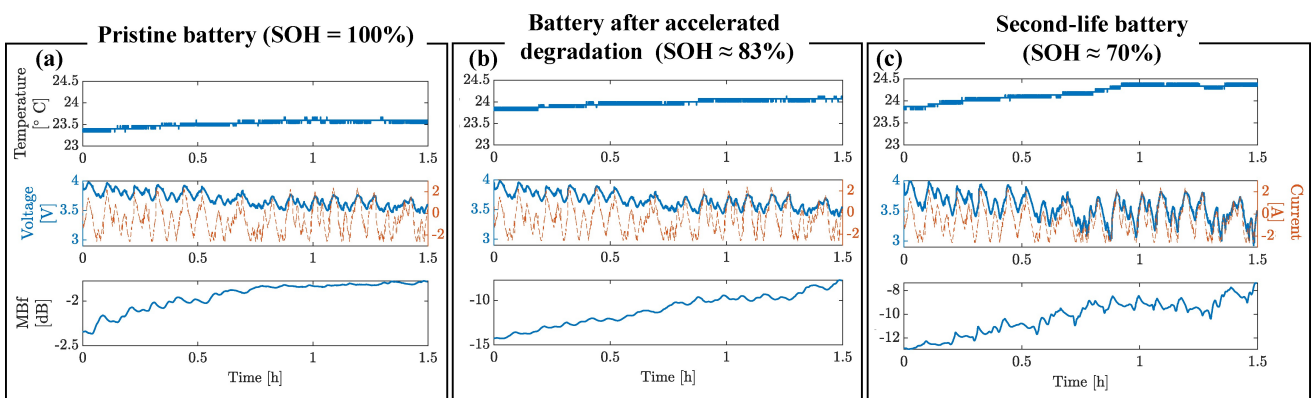


Figure 6. Temperature, applied current (dashed red), with resulting voltage (blue) and MBf values during ultrasonic testing while batteries were discharged using a current profile emulating a real drive cycle for (a) a pristine cell, (b) a cell after accelerated degradation protocol and (c) a second-life cell.

response is similar to findings from the previous sections, where a general increase in MBf was noted as the battery progressively discharged. However, these findings are part of a preliminary investigation only. Since the cylindrical geometry is significantly more complicated than other geometries, we currently limit the conclusion to noting a correlation between the MBf and the SOC in this specific context. This observation motivates future research to delve deeper into exploring, establishing and generalizing this correlation.

Conclusions

In this study, we introduced a frequency-based analysis approach employing quantitative ultrasound spectroscopy for rapid non-invasive assessment of battery health. This demonstrated the sensitivity of circumferential ultrasound waves to the state of charge (SOC) and state of health (SOH) of Li-ion batteries, offering a valuable method for evaluating the health condition of common cylindrical format cells, including 18650, 21700, 4680, and others. The method was successfully applied to pristine batteries subjected to accelerated degradation experiments as well as second-life batteries. Furthermore, we explored drive cycle scenarios where current demands are not constant and can change rapidly, demonstrating preliminary success in the context of SLBs.

The results of this study demonstrate the ability of the mid-band fit parameter to track the SOC and discriminate between different SOH levels after degradation cycling. The MBf was more sensitive to changes in the SOH at high SOC compared to measurements at low SOC. The study also shows the potential of this method to serve as a rapid assessment tool for second-life battery use in a circular economy, reducing the time required for screening from hours to microseconds, addressing a significant challenge in ultrasonic testing for assessing the SOH of batteries with unknown usage history.

This work was limited to the analysis of batteries of specific chemistry (NMC) and with cylindrical geometries, which have been less explored by other ultrasonic testing approaches. Further work will explore other battery chemistries and geo-

metries using QUS parameters. In the future, further simulation, post-mortem analysis and experimentation with other non-invasive methods will help to identify the physical mechanisms associated with changes in different ultrasonic characteristics of the QUS parameters.

Additionally, the practical application of our methodology to batteries with unknown usage history, as encountered in second-life battery scenarios, introduces uncertainties that need further exploration. Understanding the performance of the method under various usage conditions and battery chemistries is essential for its robustness and applicability.

Beyond its immediate applications, our study has broader implications, particularly in the context of a circular economy. The ability to rapidly assess the SOH of SLBs is crucial for their integration into sustainable energy storage systems. By reducing screening time from hours to microseconds, our method addresses a significant challenge in ultrasonic testing, paving the way for efficient and cost-effective utilization of SLBs.

In conclusion, while our study provides valuable insights, it paves the groundwork for future research that should address current limitations, explore alternative battery scenarios, and push the boundaries of non-invasive battery health assessment techniques.

Experimental Section

Battery Characterization and Cycling Protocols

In this study, the *operando* ultrasound response of thirteen commercially available cylindrical (model 18650) LIBs was investigated. The general characteristics of these batteries are reported in Table 1. The cells were of two types: 1) a group of 3 pristine batteries that were subjected to accelerated degradation protocols, and 2) a group of 10 SLBs, recovered by second-life battery start-up BATx SAS. The methodology presented here was tested in three scenarios, described in the following sections.

Table 1. Cell information.

Characteristic	Value
Nominal capacity	2.6 Ah
Voltage range	2.75–4.2 V
Positive electrode chemistry	NMC (Nickel-Manganese-Cobalt)
Negative electrode chemistry	Graphite
Geometry (D×H)	18.4×65.0 mm
Manufacturer reference	LG M26

Accelerated Degradation on Pristine Batteries

Three pristine batteries were subjected to 40 accelerated degradation cycles at high C-rate (2C, 5.2 A) and low temperature (5 °C) in a battery cycler (Ivium OctoBoost16000) using a constant current - constant voltage (CC-CV) charge and CC discharge protocol between the cutoff voltages in Table 1. The cutoff current for the CV phase was 0.05C. Additionally, before cycling and after cycle numbers 6, 12, 18, 24, 30, and 40, a RPT was performed at low C-rate (0.2C) and room temperature (25 °C) with CC-CV for charge and CC for discharge. During the RPT, ultrasound measurements were taken every 30 s and the SOH was assessed by Coulomb counting using the discharge capacity. All experiments were carried out in a thermal chamber (Binder MK53) with a K-type thermocouple placed on the cell surface (located as shown in Figure 7) for temperature measurements.

Testing Second-Life Batteries

The ten SLBs were cycled three times under RPT conditions at 0.2C and room temperature at 25 °C. A CC protocol was used for both the charge and discharge phases. The discharge capacity was used to assess the SOH and ultrasonic measurements were performed every 30 s. These cells were taken from a two-wheeler EV, with no record of historical usage data.

Extending the Ultrasound Methodology to a Drive Cycle Test

In order to explore the methodology proposed in this study in environments such as EV operation, where the discharge behavior is variable, a real-world driving discharge cycle was performed on three batteries: a new battery, an aged battery from the accelerated

degradation process, and a second-life battery. First, the batteries were discharged using a CC protocol to the lower cut-off voltage, followed by a CC charging phase to a final voltage of 3.95 V. Then a discharge phase emulating a driving cycle test, as used in Ref. [67], was performed while ultrasonic measurements were recorded every 4 s until the voltage reached 2.7 V.

Ultrasonic Measurements and Feature Extraction

Ultrasonic measurements were acquired using a 5 MHz center frequency and 64 – element linear array transducer (Imasonic SAS) and a Vantage 256 Research Ultrasound system (Verasonics Inc.). A pulse-echo setup was used to analyze signals from ultrasound-battery interaction. A 3D-printed case was used to perform the ultrasonic and electrochemical experiments in this study. The ultrasound array was placed longitudinally at the top of the cylindrical cell with both the cell and sensor immersed in a mineral oil (330779 Merck) bath to ensure coupling and alignment between the ultrasound probe and the battery (see Figure 7). To check if the cells self-discharged faster when immersed, a self-discharge test was performed on 2 cells by charging them using a CCCV protocol up to 4.2 V and monitoring OCV evolution for 2 days. The OCV change was negligible. Using a plane-wave imaging sequence, ten ultrasound frames were obtained at a frame rate of 1 kHz. A single ultrasound pulse as 40 V, with 5 MHz frequency symmetric broadband, was used for excitation in all the experiments.

Radio frequency (RF) data from all 64 channels were recorded at a sampling rate of 20 MHz. The data analysis was limited to the time signal between 10 µs and 11 µs (highlighted with a dotted white square in Figure 8(a)), which corresponds to the arrival time of the ultrasonic waves around the stainless steel cylindrical case. Signals were time-gated using a Hanning window to extract the region described above from each of the elements. Example time-gated signals from the 64 elements are plotted in Figure 8(b).

The windowed signals were then used to compute a power spectrum for each element, using the square magnitude of the Fourier transformed RF signal for each time series (a log-compressed representation is shown in Figure 8(c)); then all 64 power spectra were averaged to obtain a mean power spectrum, $R_{\text{avg}}(f)$. A normalized spectrum, $R_N(f)$, was then calculated using Eq. (2), with a reference spectrum $R_{\text{ref}}(f)$ taken from an empty battery case to adjust for system or acquisition dependent effects.

$$R_N(f) = 10 \log_{10} \frac{R_{\text{avg}}(f)}{R_{\text{ref}}(f)} \quad (2)$$

A line $R_{\text{linear}}(f)$ was fitted to the normalized power spectrum in the range 3.8–5.5 MHz. Figure 8(d) shows representative normalized spectra from two batteries with different SOH at a discharge condition (i.e., at 0% SOC), and their linear fits. From the fitted model, Eq. (3), the slope SS and intercept IO were extracted. The MBf corresponds to the magnitude of the fitted linear model at the middle frequency of 4.65 MHz (Eq. (4)). The motivation for extracting these parameters from a fitted model is that they can eventually be assigned a physical meaning, as has been done in previous work from biomedical applications.^[87] However, this will require further investigation to be applied to this battery case.

$$R_N(f) \approx R_{\text{linear}}(f) = SS \cdot f + IO \quad (3)$$

$$\text{MBf} = R_{\text{linear}}(f_{\text{mid}} = 4.65 \text{ MHz}) \quad (4)$$

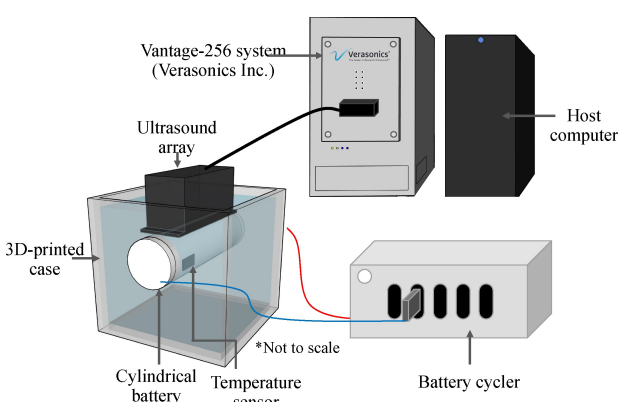


Figure 7. Overview of experimental setup, including 3D-printed case for immersion in oil to guarantee good coupling between the ultrasonic array and the cylindrical battery during cycling and ultrasound measurements.

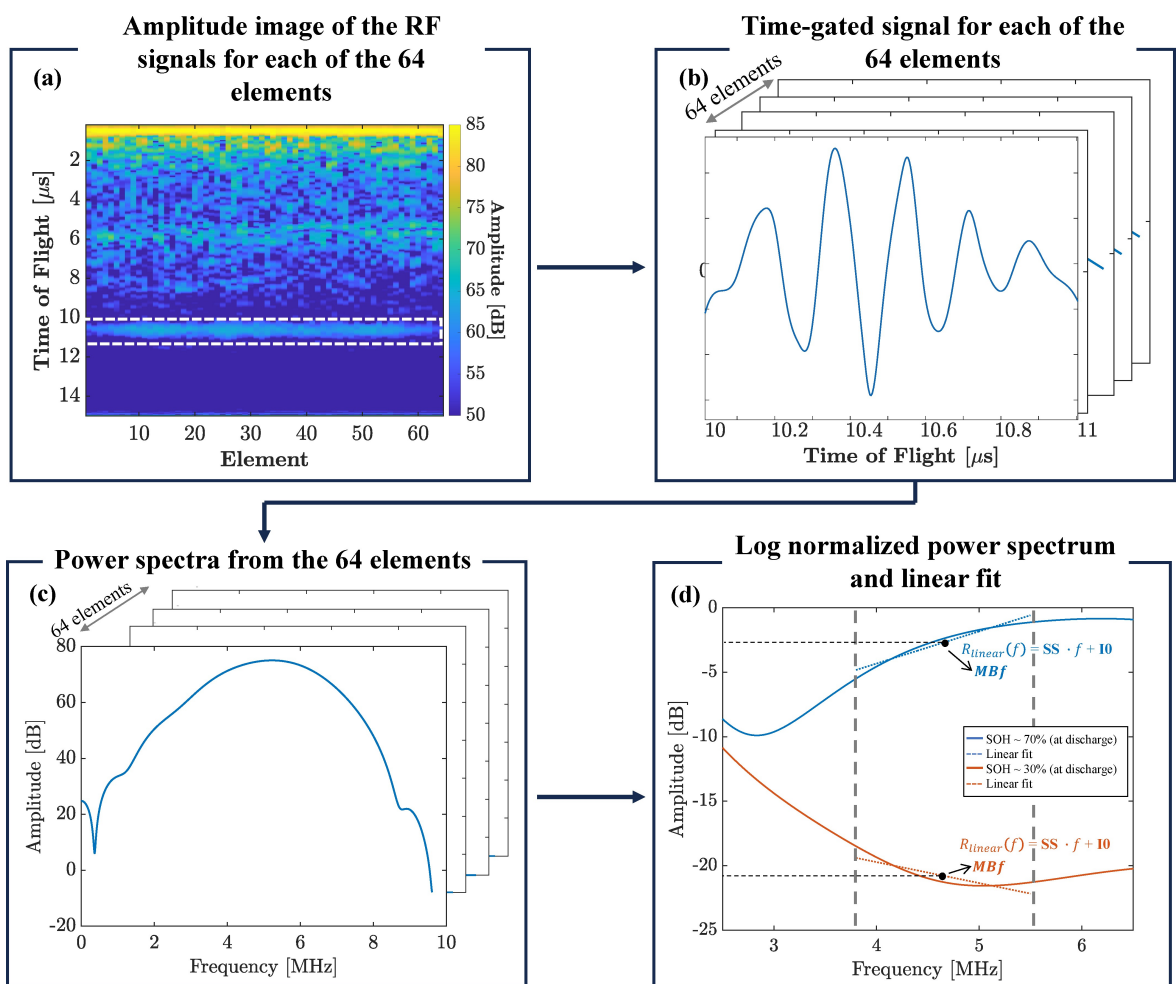


Figure 8. High-level representation of the approach used in this work to calculate the QUS parameters. (a) Example of an image of the log amplitude of the RF signal from the 64 elements of the probe showing the characteristic region analyzed, (b) time-gated signals from the characteristic zone analyzed, (c) power spectra calculated using Fourier transform and (d) normalized power spectrum with linear fit to obtain QUS parameters.

Simulation Characteristics

Ultrasound propagation simulations were conducted using SimSonic^[68] to analyze wave propagation within cylindrical batteries. SimSonic, an open-source software tool, employs a finite-difference time-domain approach. Figure 1(a) shows a schematic of the cross-section (indicated by the dotted square) employed for simulation using one element emitting and receiving (highlighted as a red square) from the ultrasonic array. As illustrated in Figure 1(b), the simulation mesh aims to replicate the transverse

section of a battery. This was achieved by modeling concentric annuli of different materials, each with unique mechanical properties (sourced from Ref. [61] under a fully-discharged condition for the NMC chemistry) and varying thicknesses, as detailed in the zoomed-in view of the different layers. The mass density ρ , the stiffness tensor with components C_{11} , C_{12} , C_{22} and C_{66} , and the thickness of each material layer were used in the simulation (see Table 2 for the used values). A detailed description of the simulation conditions and the equations used to calculate the

Table 2. Mechanical properties and thickness of the battery materials layers used in simulation.

	Density ρ (mg·mm ⁻³)	C_{11} (GPa)	C_{22} (GPa)	C_{12} (GPa)	C_{66} (GPa)	Thickness (mm)
NCM	1.54	19.39	19.39	8.31	5.54	0.058
Graphite	1.06	10.11	10.11	3.19	3.46	0.066
Aluminium current collector	2.7	103.57	103.57	51.71	25.93	0.02
Copper current collector	8.96	170.55	170.55	90.23	40.16	0.01
Separator	1.68	1.66	1.66	1.42	0.12	0.029
Stainless steel case ^[88]	7.88	204.6	204.6	137.7	126.2	0.5
Mineral oil	0.83	2.25	2.25	2.25	0.0	N/A

stiffness tensor components from the Lamé elastic constants can be found in the Supporting Information.

Supporting Information

A file containing the supplementary information, supplementary results figures (PDF), and a supplementary movie with the simulation to understand the ultrasound wave propagation in the cylindrical batteries. Additional references cited within the Supporting Information.^[68,89]

Acknowledgements

This project was supported by the Royal Academy of Engineering, through the Engineering X Transforming Systems through Partnership programme (grant number TSP2021/100333). Special acknowledgment also goes to Verasonics Inc. for providing the ultrasound equipment, and BATx for providing the second-life batteries used in this study.

Conflict of Interests

Simon Montoya-Bedoya is a Junior Ultrasound Scientist at Verasonics SAS. Esteban Garcia-Tamayo is a battery consultant at Titan Advanced Energy Solutions and Scientific Advisor at BATx. Daniel Rohrbach and Miguel Bernal are Senior Scientists of Verasonics Inc. David Howey is co-founder of Brill Power Ltd.

Data Availability Statement

The data that support the findings of this study are available from the corresponding author upon reasonable request.

Keywords: quantitative ultrasound spectroscopy · ultrasound · lithium-ion battery · state of health · second-life

- [1] IPCC, Global Warming of 1.5°C. An IPCC Special Report on the impacts of global warming of 1.5°C above pre-industrial levels and related global greenhouse gas emission pathways, in the context of strengthening the global response to the threat of climate change, 2018.
- [2] C. Xu, Q. Dai, L. Gaines, M. Hu, A. Tukker, B. Steubing, *Communications Materials* **2020**, 1.
- [3] W. Liu, T. Placke, K. Chau, *Energy Reports* **2022**, 8, 4058.
- [4] Hannah Ritchie, Pablo Rosado and Max Roser (2023) - "Energy" in Our World in Data **2022**, <https://ourworldindata.org/energy>.
- [5] Y. Yang, E. G. Okonkwo, G. Huang, S. Xu, W. Sun, Y. He, *Energy Storage Mater.* **2021**, 36, 186.
- [6] M. Etxandi-Santolaya, L. C. Casals, B. A. García, C. Corchero, *World Electric Vehicle Journal* **2023**, 14, 66.
- [7] G. Mishra, R. Jha, A. Meshram, K. K. Singh, *J. Environ. Chem. Eng.* **2022**, 10, 108534.
- [8] T. Tawonezvi, M. Nomnqa, L. Petrik, B. J. Bladergroen, *Energies* **2023**, 16, 1365.
- [9] E. Martinez-Laserna, I. Gandiaga, E. Sarasketa-Zabala, J. Badeda, D.-I. Stroe, M. Swierczynski, A. Goikoetxea, *Renewable Sustainable Energy Rev.* **2018**, 93, 701.
- [10] M. Eider, A. Berl, Dynamic EV Battery Health Recommendations, in *Proceedings of the Ninth International Conference on Future Energy Systems*, ACM **2018**.
- [11] L. C. Casals, M. Etxandi-Santolaya, P. A. Bibiloni-Mulet, C. Corchero, L. Trilla, *Batteries* **2022**, 8, 164.
- [12] M. Etxandi-Santolaya, L. C. Casals, T. Montes, C. Corchero, *J. Environ. Manage.* **2023**, 338, 117814.
- [13] E. Michelini, P. Höschele, F. Ratz, M. Stadlbauer, W. Rom, C. Ellersdorfer, J. Moser, *Energies* **2023**, 16, 2830.
- [14] J. Zhu, I. Mathews, D. Ren, W. Li, D. Cogswell, B. Xing, T. Sedlatschek, S. N. R. Kantareddy, M. Yi, T. Gao, Y. Xia, Q. Zhou, T. Wierzbicki, M. Z. Bazant, *Cell Rep. Physical Science* **2021**, 2, 100537.
- [15] X.-T. Wang, Z.-Y. Gu, E. H. Ang, X.-X. Zhao, X.-L. Wu, Y. Liu, *Interdiscip. Materials* **2022**, 1, 417.
- [16] M. F. Börner, M. H. Frieges, B. Späth, K. Spütz, H. H. Heimes, D. U. Sauer, W. Li, *Cell Rep. Physical Science* **2022**, 3, 101095.
- [17] M. H. S. M. Haram, J. W. Lee, G. Ramasamy, E. E. Ngu, S. P. Thiagarajah, Y. H. Lee, *Alexandria Eng. J.* **2021**, 60, 4517.
- [18] S. Montoya-Bedoya, L. A. Sabogal-Moncada, E. Garcia-Tamayo, H. V. Martínez-Tejada, A Circular Economy of Electrochemical Energy Storage Systems: Critical Review of SOH/RUL Estimation Methods for Second-Life Batteries, in *Green Energy and Environment*, IntechOpen **2020**.
- [19] C. R. Birk, M. R. Roberts, E. McTurk, P. G. Bruce, D. A. Howey, *J. Power Sources* **2017**, 341, 373.
- [20] J. S. Edge, S. O'Kane, R. Prosser, N. D. Kirkaldy, A. N. Patel, A. Hales, A. Ghosh, W. Ai, J. Chen, J. Yang, S. Li, M.-C. Pang, L. B. Diaz, A. Tomaszewska, M. W. Marzook, K. N. Radhakrishnan, H. Wang, Y. Patel, B. Wu, G. J. Offer, *Phys. Chem. Chem. Phys.* **2021**, 23, 8200.
- [21] O. for Product Safety & Standards, A Study on the Safety of Second-life Batteries in Battery Energy Storage Systems, Technical report, OPSS Office for Product Safety and Standards **2023**.
- [22] A. Basia, Z. Simeu-Abazi, E. Gascard, P. Zwolinski, *CIRP Journal of Manufacturing Science and Technology* **2021**, 32, 517.
- [23] J. Lee, J. Won, *IEEE Access* **2023**, 11, 15449.
- [24] D. T. Gladwin, C. R. Gould, D. A. Stone, M. P. Foster, Viability of "second-life" use of electric and hybridelectric vehicle battery packs, in *IECON 2013 – 39th Annual Conference of the IEEE Industrial Electronics Society*, IEEE **2013**.
- [25] M. Hassini, E. Redondo-Iglesias, P. Venet, *Batteries* **2023**, 9, 385.
- [26] A. Ran, S. Chen, S. Zhang, S. Liu, Z. Zhou, P. Nie, K. Qian, L. Fang, S.-X. Zhao, B. Li, F. Kang, X. Zhou, H. Sun, X. Zhang, G. Wei, *RSC Adv.* **2020**, 10, 191117.
- [27] W. Du, R. E. Owen, A. Jnawali, T. P. Neville, F. Iacoviello, Z. Zhang, S. Liard, D. J. Brett, P. R. Shearing, *J. Power Sources* **2022**, 520, 230818.
- [28] H. Villarraga-Gómez, D. L. Begun, P. Bhattacharjee, K. Mo, M. N. Rad, R. T. White, S. T. Kelly, *Nondestr. Test. Eval.* **2022**, 37, 519.
- [29] M. Zhang, Y. Liu, D. Li, X. Cui, L. Wang, L. Li, K. Wang, *Energies* **2023**, 16, 1599.
- [30] M. Faraji-Niri, M. Rashid, J. Sansom, M. Sheikh, D. Widanage, J. Marco, *J. Energy Storage* **2023**, 58, 106295.
- [31] M. Messing, T. Shoa, S. Habibi, *J. Energy Storage* **2021**, 43, 103210.
- [32] L. Wang, Z. Song, L. Zhu, J. Jiang, *iScience* **2023**, 26, 106463.
- [33] H. Popp, M. Koller, M. Jahn, A. Bergmann, *J. Energy Storage* **2020**, 32.
- [34] K. Wang, Q. Chen, Y. Yue, R. Tang, G. Wang, L. Tang, Y. He, *Nondestr. Test. Eval.* **2023**, 38, 480.
- [35] Z. Wang, K. Lu, X. Chen, D. Zhen, F. Gu, A. D. Ball, Rapid State of Health Estimation of Lithium-ion Batteries based on An Active Acoustic Emission Sensing Method, in *2022 27th International Conference on Automation and Computing (ICAC)*, IEEE **2022**.
- [36] J. O. Majasan, J. B. Robinson, R. E. Owen, M. Maier, A. N. P. Radhakrishnan, M. Pham, T. G. Tranter, Y. Zhang, P. R. Shearing, D. J. L. Brett, *Journal of Physics: Energy* **2021**, 3, 032011.
- [37] G. Davies, K. W. Knehr, B. V. Tassell, T. Hodson, S. Biswas, A. G. Hsieh, D. A. Steingart, *J. Electrochem. Soc.* **2017**, 164, A2746.
- [38] P. Ladpli, C. Liu, F. Kopsaftopoulos, F. K. Chang, Estimating Lithium-ion Battery State of Charge and Health with Ultrasonic Guided Waves Using an Efficient Matching Pursuit Technique, Institute of Electrical and Electronics Engineers Inc. **2018**.
- [39] E. Galionas, T. G. Tranter, R. E. Owen, J. B. Robinson, P. R. Shearing, D. J. Brett, *Energy and AI* **2022**, 10, 100188.
- [40] R. Gauthier, A. Luscombe, T. Bond, M. Bauer, M. Johnson, J. Harlow, A. Louli, J. R. Dahn, *J. Electrochem. Soc.* **2022**, 169, 020518.
- [41] B. Sun, C. Zhang, S. Liu, L. Jin, Q. Yang, *J. Electrochem. Soc.* **2022**, 169, 030511.

- [42] B. Sood, M. Osterman, M. Pecht, Health monitoring of lithium-ion batteries, in *2013 IEEE Symposium on Product Compliance Engineering (ISPACE)*, IEEE 2013.
- [43] A. G. Hsieh, S. Bhadra, B. J. Hertzberg, P. J. Gjeltema, A. Goy, J. W. Fleischer, D. A. Steingart, *Energy Environ. Sci.* **2015**, *8*, 1569.
- [44] L. Gold, T. Bach, W. Virsik, A. Schmitt, J. Müller, T. E. Staab, G. Sextl, *J. Power Sources* **2017**, *343*, 536.
- [45] H. Poppe, M. Koller, S. Keller, G. Glanz, R. Klambauer, A. Bergmann, *IEEE Access* **2019**, *7*, 170992.
- [46] Y. Wu, Y. Wang, W. K. Yung, M. Pecht, *Electronics (Switzerland)* **2019**, *8*.
- [47] J. B. Robinson, M. Pham, M. D. Kok, T. M. Heenan, D. J. Brett, P. R. Shearing, *J. Power Sources* **2019**, *444*.
- [48] A. Mukhopadhyay, B. W. Sheldon, *Prog. Mater. Sci.* **2014**, *63*, 58.
- [49] Y. Qi, L. G. Hector, C. James, K. J. Kim, *J. Electrochem. Soc.* **2014**, *161*, F3010.
- [50] Q. Ke, S. Jiang, W. Li, W. Lin, X. Li, H. Huang, *J. Power Sources* **2022**, *549*.
- [51] T. Hodson, S. Patil, D. A. Steingart, *J. Electrochem. Soc.* **2021**, *168*, 070515.
- [52] P. Ladpli, F. Kopsaftopoulos, F. K. Chang, *J. Power Sources* **2018**, *384*, 342.
- [53] G. Zhao, Y. Liu, G. Liu, S. Jiang, W. Hao, *J. Energy Storage* **2021**, *39*.
- [54] X. Li, C. Wu, C. Fu, S. Zheng, J. Tian, *Energies* **2022**, *15*.
- [55] G. Jie, Z. Liangheng, L. Yan, S. Fan, W. Bin, H. Cunfu, *J. Energy Storage* **2023**, *72*, 108384.
- [56] Z. Yang, H. Yang, T. Tian, D. Deng, M. Hu, J. Ma, D. Gao, J. Zhang, S. Ma, L. Yang, H. Xu, Z. Wu, *Ultrasonics* **2023**, *133*, 107014.
- [57] S. Baazouzi, N. Feistel, J. Wanner, I. Landwehr, A. Fill, K. P. Birke, *Batteries* **2023**, *9*, 309.
- [58] G. Harper, R. Sommerville, E. Kendrick, L. Driscoll, P. Slater, R. Stolkin, A. Walton, P. Christensen, O. Heidrich, S. Lambert, A. Abbott, K. Ryder, L. Gaines, P. Anderson, *Nature* **2019**, *575*, 75.
- [59] J. Gao, Y. Lyu, C. He, *J. Phys.: Conf. Ser.* **2022**, *2198*, 012015.
- [60] A. Kirchev, N. Guillet, D. Brun-Buission, V. Gau, *J. Electrochem. Soc.* **2022**, *169*, 010515.
- [61] K. Meng, X. Chen, W. Zhang, W. Chang, J. Xu, *J. Power Sources* **2022**, *547*.
- [62] H. Sun, N. Muralidharan, R. Amin, V. Rathod, P. Ramuhalli, I. Belharouak, *J. Power Sources* **2022**, *549*.
- [63] S. Montoya-Bedoya, M. Bernal, L. A. Sabogal-Moncada, H. V. Martinez-Tejada, E. Garcia-Tamayo, Noninvasive ultrasound for Lithium-ion batteries state estimation, in *2021 IEEE UFFC Latin America Ultrasonics Symposium (LAUS)*, IEEE 2021.
- [64] J. Mamou, M. L. Oelze (Editors), *Quantitative Ultrasound in Soft Tissues*, Springer International Publishing 2023.
- [65] D. Rohrbach, B. Wodlinger, J. Wen, J. Mamou, E. Feleppa, *Ultrasound in Medicine Biology* **2018**, *44*, 1341.
- [66] P. N. Goundan, J. Mamou, D. Rohrbach, J. Smith, H. Patel, K. D. Wallace, E. J. Feleppa, S. L. Lee, *Front. Endocrinol.* **2021**, *12*.
- [67] R. E. Owen, J. B. Robinson, J. S. Weaving, M. T. M. Pham, T. G. Tranter, T. P. Neville, D. Billson, M. Braglia, R. Stocker, A. A. Tidblad, P. R. Shearing, D. J. L. Brett, *J. Electrochem. Soc.* **2022**, *169*, 040563.
- [68] E. Bossy, M. Talmant, P. Laugier, *The Journal of the Acoustical Society of America* **2004**, *115*, 2314.
- [69] The Feynman Lectures on Physics Vol. II Ch. 39: Elastic Materials – feynmanlectures.caltech.edu, https://www.feynmanlectures.caltech.edu/II_39.html, [Accessed 19-02-2024].
- [70] R. Timms, S. Psaltis, C. P. Please, S. J. Chapman, *J. Mech. Phys. Solids* **2023**, *175*, 105269.
- [71] I. A. Alshaikh, D. Turhan, Y. Mengi, *European Journal of Mechanics – A/ Solids* **2002**, *21*, 811.
- [72] J. Hemmerling, J. Guhathakurta, F. Dettinger, A. Fill, K. P. Birke, *Batteries* **2021**, *7*, 61.
- [73] W. G. Neubauer, P. Uginčius, H. Überall, *Z. Naturforsch. A* **1969**, *24*, 691.
- [74] J. Greenhall, C. Hakoda, E. S. Davis, V. K. Chillara, C. Pantea, *IEEE Transactions on Ultrasonics, Ferroelectrics, and Frequency Control* **2021**, *68*, 2251.
- [75] W. Chang, R. Mohr, A. Kim, A. Raj, G. Davies, K. Denner, J. H. Park, D. Steingart, *J. Mater. Chem. A* **2020**, *8*, 16624.
- [76] W. Chang, T. Xu, D. Steingart, *J. Electrochem. Soc.* **2022**, *169*, 090530.
- [77] J. M. Reniers, G. Mulder, D. A. Howey, *J. Electrochem. Soc.* **2019**, *166*, A3189.
- [78] W. K. Chang, *Characterizing Chemo-Mechanical Behavior of Lithium Metal Batteries*, Ph.D. thesis, Princeton University 2021.
- [79] R. F. Ziesche, T. Arlt, D. P. Finegan, T. M. M. Heenan, A. Tengattini, D. Baum, N. Kardjilov, H. Markötter, I. Manke, W. Kockelmann, D. J. L. Brett, P. R. Shearing, *Nat. Commun.* **2020**, *11*.
- [80] P. Heugel, W. Märkle, T. Deich, O. von Kessel, J. Tübke, *J. Energy Storage* **2022**, *53*, 105101.
- [81] A. Jnawali, M. D. R. Kok, M. Krishna, M. A. Varnosfaderani, D. J. L. Brett, P. R. Shearing, *J. Electrochem. Soc.* **2023**, *170*, 090540.
- [82] U. Janakiraman, T. R. Garrick, M. E. Fortier, *J. Electrochem. Soc.* **2020**, *167*, 160552.
- [83] C. Bommier, W. Chang, Y. Lu, J. Yeung, G. Davies, R. Mohr, M. Williams, D. Steingart, *Cell Rep. Physical Science* **2020**, *1*.
- [84] M. Huang, N. Kirkaldy, Y. Zhao, Y. Patel, F. Cegla, B. Lan, *J. Energy Storage* **2022**, *50*.
- [85] X. Liu, Z. Deng, Y. Liao, J. Du, J. Tian, Z. Liu, Y. Shen, Y. Huang, *Phys. Chem. Chem. Phys.* **2023**, *25*, 21730.
- [86] G. Pozzato, A. Allam, L. Pulvirenti, G. A. Negoita, W. A. Paxton, S. Onori, *Joule* **2023**, *7*, 2035–2053.
- [87] L. O. Osapoetra, L. Sannachi, D. DiCenzo, K. Quiaoit, K. Fatima, G. J. Czarnota, *Translational Oncology* **2020**, *13*, 100827.
- [88] H. M. Ledbetter, *Physica Status Solidi A* **1984**, *85*, 89.
- [89] B. Lautrup, *Physics of Continuous Matter: Exotic and Everyday Phenomena in the Macroscopic World*, Taylor & Francis 2004.

Manuscript received: January 3, 2024

Revised manuscript received: February 27, 2024

Accepted manuscript online: March 1, 2024

Version of record online: April 3, 2024